Progress In Electromagnetics Research M, Vol. 35, 39–48, 2014

Efficient Multi-Objective Optimization of Frequency Selective Radome with Nonuniform Wall Thickness

Xin Ma* **and Guo-Bin Wan**

Abstract—An efficient optimization technique for frequency selective surface (FSS) radome with nonuniform wall thickness is proposed to improve the power transmission efficiency and the boresight error (BSE) of FSS radome simultaneously. The high-frequency method based on the approximate locally planar technique is used to evaluate the transmission performance of FSS radome. An efficient multi-dimensional adaptive sampling method combined with spectral domain method of moment (MoM) is employed to analyze transmission performance of FSS structure. The immune clone algorithm (ICA) is applied to the design of a FSS radome, in which the linear combination of the maximizing power transmission efficiency and the minimizing BSE is adopted as the affinity function, and the radome wall thickness is optimized. A design example for the three-dimensional tangent ogive radome with nonuniform thickness is given. The results show that the power transmission efficiency is improved significantly and the BSE of the optimal antenna-radome system is also reduced over the antenna scan volume.

1. INTRODUCTION

FSS has been used in optical and microwave field owing to its capability of spatial filters. One example of the applications is the integration of a FSS with a protective radome in stealth technology to reduce the radar cross section (RCS) of the enclosed antenna outside its operating band. The geometry of an airborne or streamlined FSS radome, largely determined by aerodynamic considerations, often leads to the broad range of incident angles along the curved radome surface. Steering the incident angle will lose the stability of the resonant frequency of FSS. Thus, the FSS radome may influence the electrical performance of the enclosed antenna, such as loss of power transmission efficiency or deflection of the antenna main beam. It is well known that the dielectric profile plays the most important role in realizing stable transmission response of FSS [1]. As a consequence, in order to improve the electrical performance of FSS radome, effective optimization of dielectric thickness for different incident angles along the curved radome surface is necessary.

In recent years, much more optimization strategies concentrate on the optimization of planar FSS structures. There are several publications in which genetic algorithm (GA) or its counterparts, such as the micro-genetic algorithm (MGA), have been applied to find patch shapes with the best performance [2–4]. Chakravarty and Mittra present a procedure for synthesizing single and multilayered FSS screens embedded in multilayered dielectric media at near-grazing angles of incidences via MGA [3]. A modal-based parameter estimation is introduced in GA aided FSS design [4]. The particle swarm optimization (PSO) is an evolutionary computation technique inspired by social behavior of a flock of birds and insect swarms. It has been introduced to the synthesis of infinite planar FSS structure [5] and design of planar FSS-equipped radome [6]. Clone selection algorithm is one of the many branches

Received 25 December 2013, Accepted 18 February 2014, Scheduled 21 February 2014

* Corresponding author: Xin Ma (maxine1105@163.com).

The authors are with the School of Electronics and Information, Northwestern Polytechnical University, Xi'an, Shaanxi 710129, P. R. China.

of the artificial immune system algorithms that has recently drawn considerable attention in a wide range of applications [7]. It has been shown that the clone selection algorithm is very effective on multimodal problems due to its inherent properties [8]. A real-valued parallel clone selection algorithm was successfully applied in optimization of multi-layered planar FSS [9]. From the low number of manuscripts published, it seems that there is lack of an efficient method for the curved FSS radome optimization, owing to complex and tremendous computational burden.

For practical antenna-FSS radome systems, the full wave analysis is usually unaffordable due to the excessive computation. Thus, high-frequency method based on the approximate locally planar technique method is required for an approximate description [10–13]. The incidence angles continuously vary along the curved radome surface. If the scattering properties of the planar selective structure for arbitrary incidences are obtained only by means of a full-wave method, it would be unfeasible to analyze the FSS radome, not to mention the optimization. An efficient solution to this problem is provided by the method of multi-dimensional adaptive sampling method (ASM) [14], which allows one to obtain the electromagnetic characteristics of FSS for multi-dimensional parameter space more efficiently.

An efficient method to optimize the radome-wall thickness profile for curved FSS radome is proposed in this paper. The paper is organized as follows. The design problem for FSS radome is briefly summarized in Section 2. In Section 3, the electromagnetic performance of the antenna-radome system is determined by the high-frequency method, and combined with spectral domain MoM, the multi-dimensional ASM is employed to evaluate the transmission performance of FSS efficiently. The immune clone algorithm (ICA) is presented in Section 4. A design example for the three-dimensional tangent ogive radome is given and the obtained results are presented in Section 5. Finally, conclusions are drawn in Section 6.

2. POSING THE DESIGN PROBLEM

Figure 1 depicts cross-sectional view of a general FSS radome and its global coordinate system. The FSS cells are arranged periodically along the cross-sectional generatrix with the local coordinate system (x, y, z) placed at the FSS cell center. L_a is the gimbal arm length. The scan angles of the antenna about the radome axis is θ. The parameters of FSS radome, such as the parameters of FSS array, the number and the thickness of dielectric layers etc., are degrees of freedom for the optimization. Considering that any function can be represented as digital sample series, these parameters of FSS radome are defined as a vector $\vec{X}$. The assessment functions of the power transmission efficiency, boresight error, etc. of FSS radome can be expressed as A_g $(g = 1, 2, \ldots, G)$ with lower limit L_g or upper limit U_g. The optimization problem for the electrical performance of FSS radome is to find the appropriate resolution $\vec{X}_{\text{opt}}$ to make the performance indicators of FSS radome fulfill a request. The optimization problem is formulated as

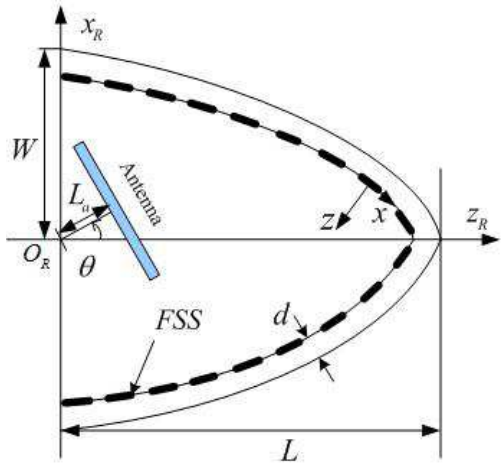

Figure 1. Cross-sectional view of three-dimensional antenna-FSS radome system.

a nonlinear programming model:

$$F\left(\vec{X}\right) = \int_{\Lambda} \xi(f) \int_{\Theta} \eta(\theta) \sum_{g=1}^{G} \left[w_g A_g \left(\vec{X}, \theta, f\right)\right] d\theta\, df \max(or\ \min) \left\{ F\left(\vec{X}\right) :\ \vec{X} \in D_X \right\} \quad L_g \leq A_g \leq U_g \quad (1)$$

where $\xi(f)$ and $\eta(\theta)$ are weighting functions for the range of operating frequency and the antenna scan angle respectively. Θ is the antenna scan volume and Λ the range of operating frequency. w_g is weighted coefficients for different A_g.

For the optimization of radome with nonuniform wall thickness, the thickness of dielectric layer is chosen as major degree of freedom for the optimization under the premise that other parameters remain unchanged. The thickness profile is parameterized as $d(\vec{s})$ corresponding to location at $\vec{s}$ on the radome surface. A realistic way is to use sampling method that the nonuniform thickness of radome wall at selected positions s_p $(p = 1, 2, \ldots, N_p)$ is chosen as the discrete thickness profile $d(s_p)$. Therefore, $\vec{X} = [d(s_1), d(s_2), \ldots, d(s_{N_p})]^t$.

For the optimization problem of power transmission efficiency and the boresight error, the objective is to search for the best possible thickness profile $\vec{X}$ to maximize the power transmission efficiency $P(\vec{X}, \theta, f)$ and minimize the BSE $\delta(\vec{X}, \theta, f)$. Therefore, the Eq. (1) can be represented as:

$$\begin{aligned} F \ = \ & \int_{\Lambda} \xi(f) \int_{\Theta} \eta(\theta) \left\{ w_1 \min \left[P\left(\vec{X}, \theta, f\right)\right] + w_2 \left\{ 1 - \max \left[\delta\left(\vec{X}, \theta, f\right)\right]\right\}\right\} d\theta\, df \\ & \max \left\{ F:\ \left| d(s_p) - d^0 \right| \leq \varepsilon \right\} \qquad\qquad P\left(\vec{X}, \theta f\right) \geq P_{\min}, \quad \delta\left(\vec{X}, \theta f\right) \leq \delta_{\max} \end{aligned} \quad (2)$$

where $P_{\min}$ is the minimal power transmission efficiency, $\delta_{\max}$ the maximal boresight error, d^0 the initial thickness which can be the thickness of uniform radome, and ε a constant determining the range of $d(s_p)$. The problem is reduced to a standard form of multidimensional global optimization.

3. SOLVING TRANSMISSION PERFORMANCE OF RADOME BASED ON ASM

In view of computational efficiency, the physical optics approach, which can get acceptable results for the analysis of radome with smooth and large curvature radius surface [13, 15], is adopted. The field radiate from the aperture of the antenna is assumed as a Huygens' source and transmits through the FSS radome. The curved frequency selective structure is replaced by the tangent locally planar one at the incidence point s_p. The transmitted field on the outer surface is calculated from the infinite inductive FSS analysis with the plane of the FSS positioned tangent to the surface at each location. Once the transmitted fields on the outer surface are found, the fields the equivalent electric and magnetic currents can be obtained. Finally, the Stratton-Chu formulation is adopted to determine the radiation performances of the antenna-radome system in the far region. The power transmission efficiency and the boresight error can be derived. The crux of the problem is how to receive the transmission characteristic of the tangent locally planar frequency selective structure.

The direction of incidence is $(\theta_p^i, \varphi_p^i)$ which is defined by projecting the propagation vector to the surface normal of FSS radome at each position s_p [15]. The incident fields and the induced currents on the conducting surfaces for an infinite planar array with periodicities T_x and T_y in x, y directions are related as:

$$-\mathbf{E}^i(x, y) = \frac{1}{T_x T_y} \sum_{\alpha=-\infty}^{\infty} \sum_{\beta=-\infty}^{\infty} \tilde{\tilde{G}} \tilde{J}\left(k_{x\alpha} k_{y\beta}\right) e^{jk_{x\alpha}x} e^{jk_{y\beta}y} \quad (3)$$

where $\mathbf{E}^i$ represents the incident filed, and $\tilde{\tilde{G}}$ denotes the pertinent dyadic Green's function [16] in the spectral domain which is related with the parameters of FSS structure. $k_{x\alpha}$ and $k_{y\beta}$ are Flouqet wavenumber in x, y directions and defined by

$$k_{x\alpha} = \frac{2\alpha\pi}{T_x} + k_0 \sin\theta_p^i \cos\varphi_p^i, \qquad k_{y\beta} = \frac{2\beta\pi}{T_y} + k_0 \sin\theta_p^i \sin\varphi_p^i \quad (4)$$

where k_0 is the free-space wavenumber.

The induced current on the perfectly conduct is expanded into the RWG basis functions [17]. Through application of Galerkin's technique, Eq. (3) can be discretized into the following linear equation

$$[Z_{mn}] \cdot [I_n] = [V_m] \quad (n,\ m = 1, 2, \ldots, M_{\mathrm{b}}) \tag{5}$$

where I_n is unknown coefficient. The elements of impedance matrix and voltage vector are

$$Z_{mn} = \tilde{f}^*_{xm}\tilde{G}_{xx}\tilde{f}_{xn} + \tilde{f}^*_{xm}\tilde{G}_{xy}\tilde{f}_{yn} + \tilde{f}^*_{ym}\tilde{G}_{yx}\tilde{f}_{xn} + \tilde{f}^*_{ym}\tilde{G}_{yy}\tilde{f}_{yn} \tag{6}$$

$$V_m = E^i_x\tilde{f}^*_{xm} + E^i_y\tilde{f}^*_{ym} \tag{7}$$

where $\tilde{f}$ denotes the Fourier transforms of RWG basis functions.

Once Eq. (5) is solved, the scattering fields E^s radiated by the conducting screens can be obtained through $\tilde{\tilde{G}}$. Then the scattering parameters of FSS can be found rather easily. The transmission coefficients of TE and TM polarization are represented as

$$S^{TE} = \frac{j\left(k_{y\beta}E^+_x - k_{x\alpha}E^+_y\right)}{\left(k^2_{x\alpha} + k^2_{y\beta}\right)} \tag{8}$$

$$S^{TM} = \frac{\left(k_{x\alpha}E^+_x + k_{y\beta}E^+_y\right)}{\left(k^2_{x\alpha} + k^2_{y\beta}\right)\gamma_{\alpha\beta}/\omega\varepsilon} \tag{9}$$

where $\gamma_{\alpha\beta}$ is the Flouqet wavenumber in the z directions, and E^+ is a sum of the transmission fields radiated by the conducting screens and the transmission fields of the incident wave through the dielectric structures with all the conducting screens removed.

The transmission coefficients of FSS structure, which are related with the direction of incidence and the thickness of dielectric layers, are defined as $S(d(s_p), \theta^i_p, \varphi^i_p)$. In order to obtain the radiation performances of the antenna-radome system, it is required to solve $S(d(s_p), \theta^i_p, \varphi^i_p)$ at every position s_p. The computation time for the direct MoM simulation of FSS radome is proportional to the number of discrete positions on the radome. However, there are generally thousands of discrete positions for electrically large radome. Therefore, it will be time-consuming to get $S(d(s_p), \theta^i_p, \varphi^i_p)$ by traditional MoM. In order to eliminate repetitive computation, one effective method is the multi-dimensional ASM to interpolate the complex valued transmission efficiency of FSS radome-wall structure through multi-dimensional rational function

All variables affecting the transmission characteristics of FSS structure, for instance the direction of incidence, geometric parameters of FSS, the thickness and permittivity of dielectric slab, can be expressed as a vector (x_1,x_2, …, x_N)^t in N-dimensional parameters space and the relationship with transmission parameters can be expressed as a multi-dimensional rational function $S(x_1$,x_2, …, $x_N)$ defined as

$$S(x_1, x_2, \ldots, x_N) = \frac{a_0 + \sum_{j=1}^{M} a_j \left(\prod_{i=1}^{N} x_i^{\mu_i(j)}\right)}{b_0 + \sum_{j=1}^{D} b_j \left(\prod_{i=1}^{N} x_i^{\upsilon_i(j)}\right)} \tag{10}$$

where $\mu_i(j)$ and $\upsilon_i(j)$ are integer functions of j and represent orders of parameters x_i in numerator and denominator polynomials respectively. a and b are unknown coefficients. To determine the unknown coefficients of rational function, the numerical error for the linear equation system of Eq. (10) is always caused because of the resultant ill-conditioned coefficient matrix whose inverse is inevitable. To avoid coefficients matrix inversion, the Eq. (10) can be solved through the interpolation on tabulated data in a recurrence manner.

In the interpolation method, it is necessary to find some support points for tabulated data. Let $[x_i^{\min}, x_i^{\max}]$ denote the calculating rang of the ith-dimensional parameter x_i ($i = 1, 2, \ldots, N$). The possible points x^p_{i,t_i} ($t_i = 1, 2, \ldots, T_i$) scatter in all range of $[x_i^{\min}, x_i^{\max}]$ with sufficiently fine space.

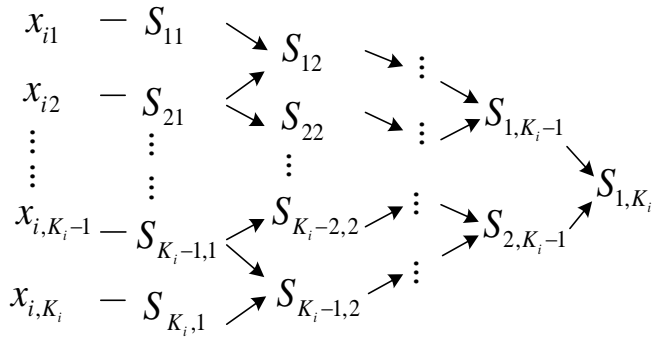

Figure 2. The tabular chart of the S-B algorithm.

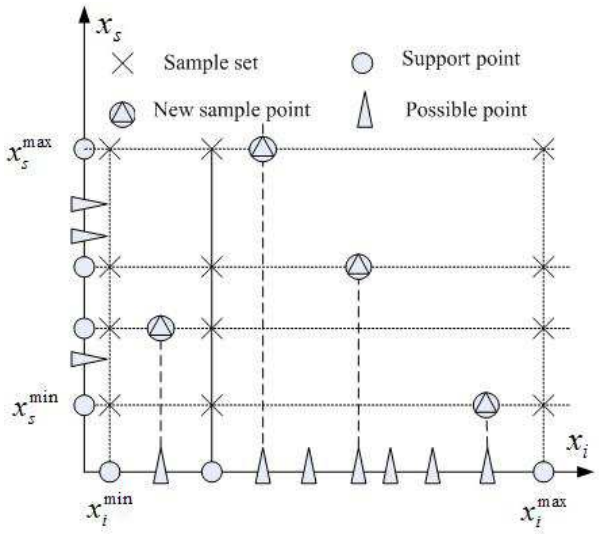

Figure 3. Finding new sample points.

x^s_{i,k_i} $(k_i = 1, 2, \ldots, K_i)$ are the support points for x_i. Perform the interpolation on tabular chart in a recurrence manner analogous to the S-B algorithm of the Neville-type [18], as shown in Fig. 2. In the initializing process, let K_i to be 2. Then the values of scattering parameters $S_{j1}(x_i)$ $(j = 1, 2, \ldots, K_i)$ which are calculated by the MoM at $x^s_{i1} = x_i^{\min}$, $x^s_{i2} = x_i^{\max}$ are used as the initializing value of the first column in tabular chart. Let x_i to be every x^p_{i,t_i} for the ith-dimensional parameter, implement interpolation as tabular chart at every constant x^s_{s,k_s} $(s = 1, 2, \ldots, N,$ but $s \neq i)$ along the x_i-axes, as shown in Fig. 3. The recurrent rules for $S_{j,l}$ $(l = 1, 2, \ldots, K_i)$ in Fig. 2 are as follow:

$$S_{j,l}\left(x_i \left| x^s_{s,k_s}, s = 1, 2, \ldots, N, \text{ but } s \neq i\right.\right) = \frac{\left(x_i - x^s_{i,j}\right) S_{j+1,l-1}(x_i) + \left(x^s_{i,j+l} - x_i\right) S_{j,l-1}(x_i)}{x^s_{i,j+l} - x^s_{i,j}} \tag{11}$$

$$S_{j,l}\left(x_i \left| x^s_{s,k_s}, s = 1, 2, \ldots, N, \text{ but } s \neq i\right.\right) = \frac{x^s_{i,j+l} - x^s_{i,j}}{\frac{x_i - x^s_{i,j}}{S_{j+1,l-1}(x_i)} + \frac{x^s_{i,j+l} - x_i}{S_{j,l-1}(x_i)}} \tag{12}$$

$$S_{j,l}\left(x_i \left| x^s_{s,k_s}, s = 1, 2, \ldots, N, \text{ but } s \neq i\right.\right) = S_{j+1,l-2}(x_i) + \frac{x^s_{i,j+l} - x^s_{i,j}}{\frac{x_i - x^s_{i,j}}{S_{j+1,l-1}(x_i) - S_{j+1,l-2}(x_i)} + \frac{x^s_{i,j+l} - x_i}{S_{j,l-1}(x_i) - S_{j+1,l-2}(x_i)}} \tag{13}$$

By using a distinct combination of the three recursive rules Eqs. (11)–(13) in association with a step sequence, an analytical function implemented along a path establishes a rational function model. There are two approximate rational function models required in each of iterative steps. With the increase of the number of samples, two approximate models will be close to each other until the convergence error satisfies a termination criterion. At the areas of highest error of iterative process, x^p_{i,t_i} would be a new support point and K_i add 1. The new support points in each dimension are chosen in adaptive way until the difference between the rational function value from interpolation and the actual sampling value from the MoM satisfies a given error tolerance. The support points must completely fill grid of points which do not have to be equidistant. The full set is given by the Cartesian product of the support points for each variable

$$(x_{11}, x_{12}, \ldots, x_{1K_1}) \times (x_{21}, x_{22}, \ldots, x_{2K_2}) \times \ldots \times (x_{N1}, x_{N2}, \ldots, x_{NK_N}) \tag{14}$$

In order to receive the objective function value $S(x_1^*, x_2^*, \ldots, x_N^*)$ at a given point $(x_1^*, x_2^*, \ldots, x_N^*)$, it needs to conduct N-dimension recursive interpolation. Set x_i in Eqs. (11)–(13) be x_i^*, and implement recursive interpolation as tabular chart at every constant $x_{s,k_s}^s (s = 1, 2, \ldots, N$ but $s \neq i)$ along the x_i-axes. The last interpolation in one dimension hands the result of its interpolation to next dimension as initializing value. The recursive interpolation is terminated with processes that interpolate from known sample points.

In the computation of the transmitted field for FSS radome, the ASM is applied to efficiently derive the transmission coefficients of FSS under different incident angles and different thickness of dielectric. Let x_1 and x_2 in Eq. (10) be the incident angle θ_p^i and φ_p^i for the locally planar FSS respectively and set x_3 to be the thickness of dielectric $d(s_p)$. The transmission response of FSS $S(d(s_p), \theta_p^i, \varphi_p^i)$ can be obtained in the recursive way.

4. IMMUNE CLONE ALGORITHM

The immune clone algorithm starts with the generation of an initial population that is consisted of N^a possible solutions of thickness profile $\vec{X}_u$ $(u = 1, 2, \ldots, N^a)$. The affinity function is defined as

$$F'\left(\vec{X}_u\right) = w_1 \min\left[P\left(\vec{X}_u, \theta, f\right)\right] + w_2\left\{1 - \max\left[\delta\left(\vec{X}_u, \theta, f\right)\right]\right\} \tag{15}$$

Each of these individuals receives a number of copies proportional to its affinity. Then the clone population $\vec{X}_v^c$ $(v = 1, 2, \ldots, N^c)$ generate. Gaussian Mutation (GM) and Cauchy Mutation (CM) which retain diversity within the population have been successfully applied in genetic algorithm [19]. In this paper, hypermutation process consists of GM and CM strategies according to the arithmetic mean of affinity function ($AMAF$) to avoid falling into local optimal solution. A clone $\vec{X}_v^c$ is altered stochastically at a certain percentage (Pr) and undergo as:

$$X_v^{c''}(p) = X_v^c(p) + \sigma_p \Delta_p \quad (p = 1, 2, \ldots, N_p) \tag{16}$$

where σ is standard deviation. If the affinity of clone molecule selected random is lower than $AMAF$, Δ is Cauchy random variable calculated by one-dimensional Cauchy density function [19]. If the affinity of clone molecule selected random is larger than $AMAF$, the mutation process undergo GM which is mutates in a small step mutation. Δ is Gaussian random variable by standard Gaussian density function. In addition to hypermutation, a part of the low affinity members are deleted and replaced by newly generated members [6]. This promotes the introduction of diverse members to the population, particularly if they achieve better affinity.

5. NUMERICAL RESULTS

5.1. Verification of ASM

In order to demonstrate the feasibility of applying the ASM to analysis of FSS, the FSS structure described as Fig. 1 in [20] is chosen. Fig. 4 shows the comparison of the transmission coefficients between the direct MoM, one-dimension ASM and experimental results given by [20]. Excellent agreement between these results has been achieved. The direct MoM responses are smoothed with 130 support points of equal space, whereas the responses of the ASM are interpolated by a rational function obtained only by 36 support samples, as shown in Fig. 4. All the computation is carried out on an Intel Core2 Duo CPU 2.4 GHz and 2.0 GB personal computer. The CPU time to obtain accurate results is 1.5 CPU hours for direct MoM calculation but only 0.45 CPU hours for ASM calculation.

To test the accuracy of $S(d(s_p), \theta_p^i, \varphi_p^i)$ solved by multi-dimension ASM described in Section 3, the transmission coefficients of the FSS structure which consists of aperture-type ring elements on a dielectric layer, as shown in Fig. 5, are calculated over wide range of d, θ^i and φ^i. The ring width is $w_r = 0.3$ mm and radius is $r = 3.09$ mm. The periodicity is $T_x = T_y = 7.24$ mm. The permittivity of dielectric slab is 3.5 and the tangent loss is 0.003. The transmission characteristic of the ring FSS is investigated under 11 GHz incident wave with changing of incident angle and d. The testing ranges of θ^i are from 15° to 75° according to the incident angles for FSS along the curved radome surface. Owing

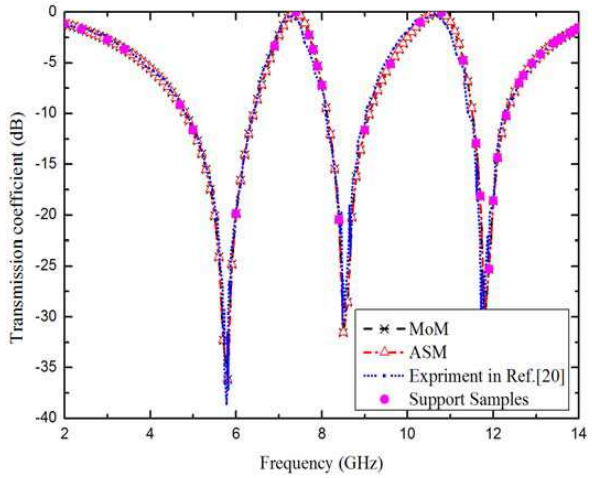

Figure 4. Frequency response of FSS in [20] under a normal incidence.

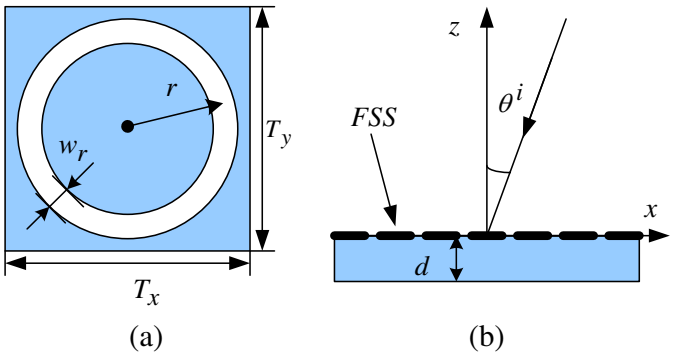

Figure 5. Geometry of ring FSS array on a dielectric slab. (a) Top view of a cell. (b) Side view.

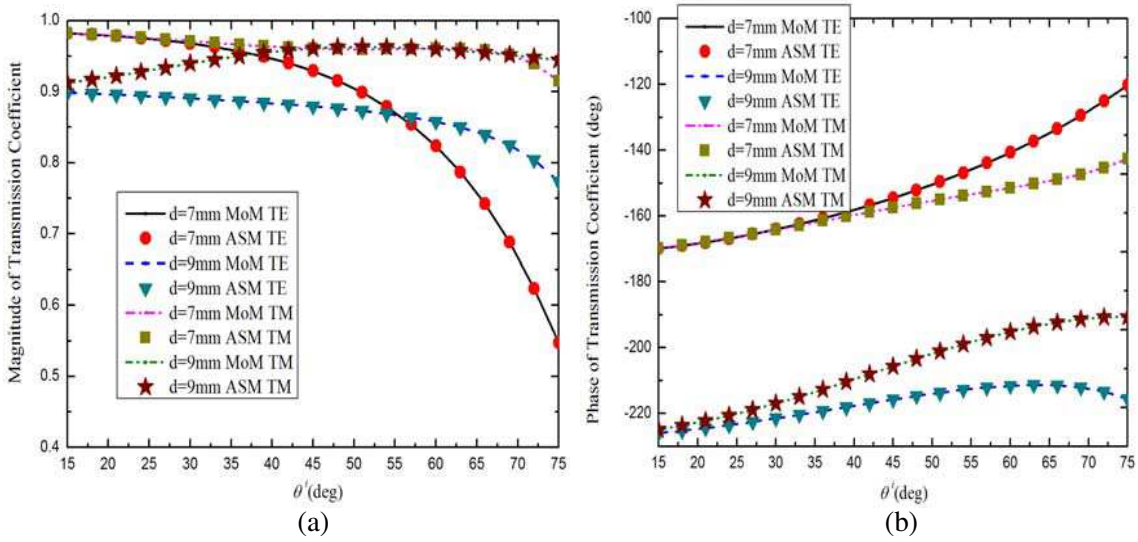

Figure 6. Transmission coefficient of ring FSS at $f = 11\,\text{GHz}$ and $\varphi^i = 24°$. (a) Magnitude of transmission coefficient. (b) Phase of transmission coefficient.

to symmetry of ring element, the testing ranges of φ^i are from 0° to 45°. The thickness of dielectric slab $d \in [5.5, 10]$ (unit: mm).

For the comparison, both results of the direct MoM and the multi-dimension ASM are shown in Fig. 6 and Fig. 7. Fig. 6 shows the transmission coefficients of the FSS structure illuminated by an incidence wave at $f = 11\,\text{GHz}$ and $\varphi^i = 24°$ for $d = 7\,\text{mm}$, 9 mm. Fig. 7 depicts the transmission coefficients of the FSS when $d = 7.87\,\text{mm}$ under an incidence wave at $f = 11\,\text{GHz}$ and $\varphi^i = 10°$, 30°. As seen, the model of ASM simulation is in very good agreement with the MoM simulated result. It takes only 1.2 CPU hours by multi-dimension ASM method to solve $S(d, \theta^i, \varphi^i)$, but it requires 56 hours by direct MoM to obtain the same information.

To validate the feasibility of applying the ASM to analysis of FSS radome, Fig. 8 shows the measured plane wave transmission response of an FSS manufactured with ring slot elements in [12] compared with the result predicted by the proposed method in this paper. The FSS was curved into a parabolic cylinder of focal length 10 mm and aperture size 140 mm. The two curves show good agreement. Very small focal length of parabolic cylinder results in high loss.

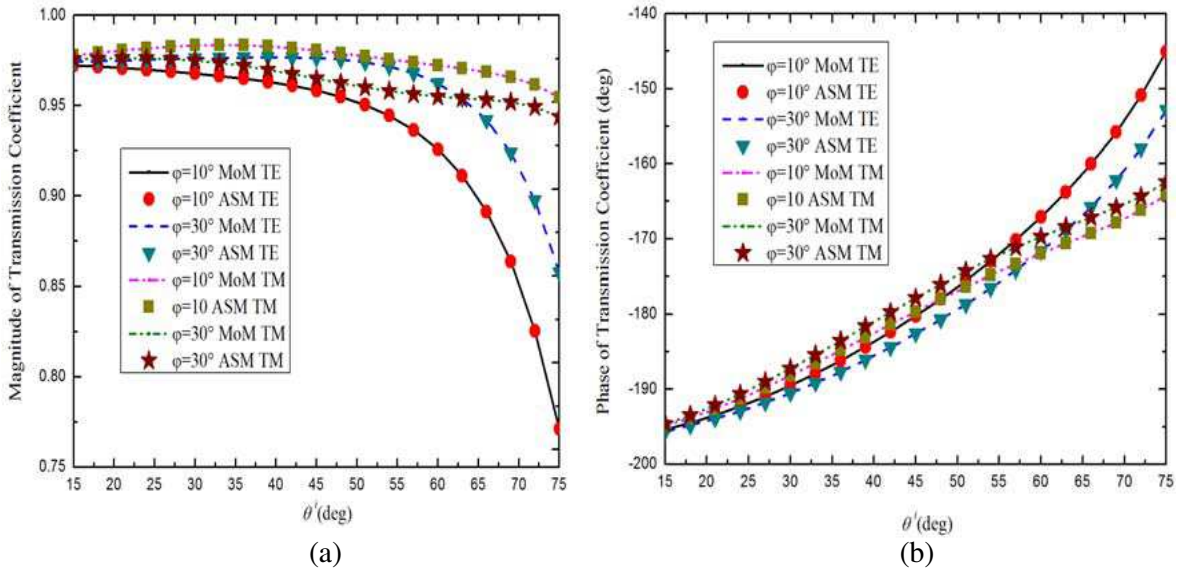

(a) (b)

Figure 7. Transmission coefficient of ring FSS with $d = 7.87\,\text{mm}$ at $f = 11\,\text{GHz}$. (a) Magnitude of transmission coefficient. (b) Phase of transmission coefficient.

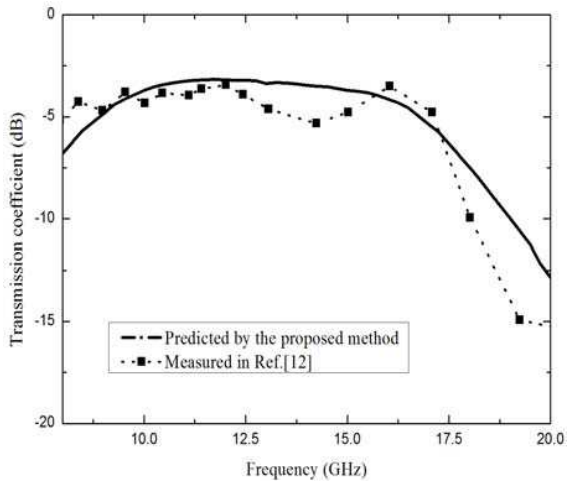

Figure 8. Power transmission response of parabolic cylindrical FSS in [12].

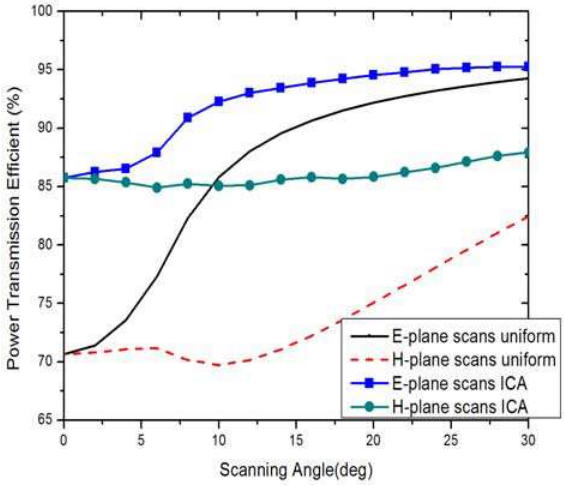

Figure 9. Power transmission efficiency for E-plane and H-plane scans.

5.2. Optimization of Nonuniform Wall Thickness

A design example is three-dimensional tangent ogive radome of revolving symmetry with a material of dielectric constant 3.5 and the tangent loss is 0.003. As shown in Fig. 1, the parameters are $L = 40\lambda$, $W = 20\lambda$, $L_a = 10\lambda$. λ is wavelength in free space. The operating frequency is 11 GHz. The antenna is a circular aperture with radius $r_a = 5\lambda$. The antenna is assumed to be a uniform linear polarized distribution.

The FSS screen is loaded on the inner surface of radome. The aperture-type ring FSS structure same with Fig. 5 is investigated. The initial substrate parameters d^0 of FSS structure were optimized with respect to the maximum magnitude of transmission coefficient illuminated by an 11 GHz 45° oblique incident wave. The initial design process is accomplished with the results of $d^0 = 7.87\,\text{mm}$.

The thickness profile function is investigated by ICA. In the ICA process, the utilized parameter values were $N_p = 15$, $Pr = 70\%$, $w_1 = 5/6$, $w_2 = 1/6$. The scan angles θ are from 0° to 30° with

2.5° step. $S(d, \theta^i, \varphi^i)$ in Section 5.1 is employed. Fig. 9 shows the power transmission efficiency against gimbal angles for E-plane and H-plane scans. As a reference, the power transmission efficiency of uniform thickness radome with $d^0 = 7.87\,\text{mm}$ are also shown in Fig. 9. In the case of uniform thickness, the power transmission efficiency has a lowest level of 70% at an antenna look direction near 0°. After optimization, it is improved to 86% maximum, a significant improvement as compared to the case of uniform thickness. The BSE against gimbal angles for E-plane and H-plane scans are shown in Fig. 10. It shows that the BSE of the optimal antenna-radome system is reduced from 0.3° to 0.07°. The resulting optimal thickness profile function is given in Fig. 11.

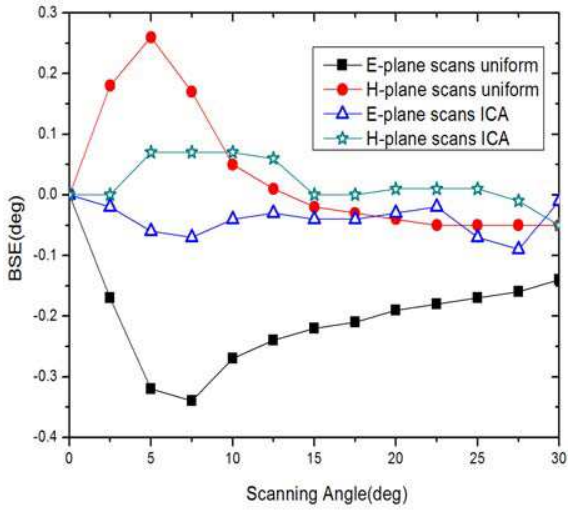

Figure 10. BSE of the uniform thickness and optimized radome by ICA.

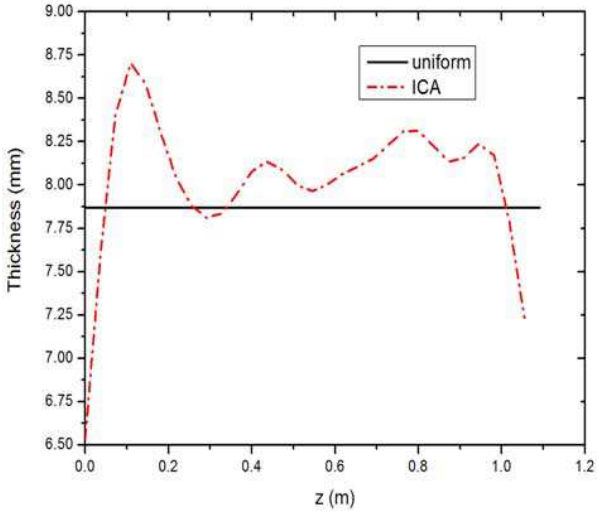

Figure 11. Optimized thickness profile functions.

6. CONCLUSIONS

For the multi-objective optimization problem of FSS radome, the ICA combined with high-frequency method and ASM is proposed to optimize the power transmission efficiency and the BSE simultaneously. Two FSS structures with different shape elements are investigated by multi-dimension ASM. The results using multi-dimension ASM compare very well to electromagnetic simulation by the direct MoM. The successful completion of a realistic design example of a tangent ogive radome with circular ring FSS is given. After entire thickness optimization, the power transmission efficiency is improved significantly and the BSE of the optimal antenna-radome system is also reduced over the antenna scan volume as a result of adjusting the thickness. It is found that the proposed method offers tremendous computational savings in terms of CPU time that makes it possible to analyze and design FSS radome more efficiently. The proposed technique has been demonstrated as a powerful approach for curved FSS radome design.

ACKNOWLEDGMENT

This work is supported by the Doctorate Foundation of Northwestern Polytechnical University (Grant No. CX201115) and by Science Foundation of Aeronautics (Grant No. 20101853019).

REFERENCES

1. Callaghan, P., E. A. Parker, and R. J. Langley, "Influence of supporting dielectric layers on the transmission properties of frequency selective surfaces," *IEE Proceedings — H*, Vol. 138, 448–454, 1991.

2. Ohira, M., H. Deguchi, M. Tsuji, et al., "Multiband single-layer frequency selective surface designed by combination of genetic algorithm and geometry-refinement technique," *IEEE Trans. Antennas Propag.*, Vol. 52, 2925–1843, 2004.
3. Chakravarty, S. and R. Mittra, "Application of the microgenetic algorithm to the design of spatial filters with frequency selective surfaces embedded in dielectric media," *IEEE Trans. on Electromagn. Compat.*, Vol. 44, 338–346, 2002.
4. Ling, L., D. H. Werner, J. A. Bossard, and T. S. Mayer, "A model-based parameter estimation technique for wide-band interpolation of periodic moment method impedance matrices with application to genetic algorithm optimization of frequency selective surfaces," *IEEE Trans. on Antennas Propag.*, Vol. 54, 908–924, 2006.
5. Genovesi, S., R. Mittra, A. Monorchio, and G. Manara, "Particle swarm optimization for the design of frequency selective surfaces," *IEEE Antennas and Wireless Propagation Letters*, Vol. 5, 277–279, 2006.
6. Sabielny, M., "Design of frequency selective radomes using parallel particle swarm optimization," *First European Conference on Antennas and Propagation*, 1–6, 2006.
7. Hart, E. and J. Timmis, "Application areas of AIS: The past, the present and the future," *Appl. Soft Comput.*, Vol. 8, 191–201, 2008.
8. Campelo, F., F. G. Guimaraes, H. Igarashi, and J. A. Ramirez, "A clone selection algorithm for optimization in electromagnetics," *IEEE Trans. on Magnetics*, Vol. 41, 1736–1739, 2005.
9. Zikri, B., A. B. Jeremy, X. D. Wang, and H. W. Douglas, "A real-valued parallel clonal selection algorithm and its application to the design optimization of multi-layered frequency selective surfaces," *IEEE Trans. Antennas Propag.*, Vol. 60, 1831–1843, 2012
10. Caroglanian, A. and K. J. Webb, "Study of curved and planar frequency-selective surfaces with nonplanar illumination," *IEEE Trans. Antennas Propag.*, Vol. 39, 211–217, 1991.
11. Martini, E., F. Caminita, M. Nannetti, et al., "Fast analysis of FSS radome for antenna RCS reduction," *IEEE Antennas and Propagation Society International Symposium*, 1801–1804, 2006.
12. Philips, B., E. A. Parker, and R. J. Langley, "Ray tracing analysis of the transmission performance of curved FSS," *IEE Proc. Microw. Antennas Propag.*, Vol. 142, 193–200, 1995.
13. D'Elia, U., G. Pelosi, C. Pichot, S. Selleri, and M. Zoppi, "A physical optics approach to the analysis of large frequency selective radomes," *Progress In Electromagnetic Research*, Vol. 138, 537–553, 2013.
14. Ma, X., G. B. Wan, and W. Wan, "A multi-dimensional adaptive sampling method for analysis and design of frequency selective surface with arbitrary element," *Progress In Electromagnetic Research B*, Vol. 41, 213–230, 2012.
15. Kozakoff, D. J., *Analysis of Radome-enclosed Antennas*, Artech House, Boston, London, 2010.
16. Wu, T. K., *Frequency Selective Surface and Grid Array*, John Wiley & Sons, New York, 1995.
17. Rao, S. M., D. R. Wilton, and A. W. Glisson, "Electromagnetic scattering by surface of arbitrary shape," *IEEE Trans. Antennas Propagat.*, Vol. 30, 409–418, 1982.
18. Stoer, J. and R. Bulirsch, *Introduction to Numerical Analysis*, Spring-Verlag, Berlin, 1980.
19. Yao, X. and Y. Liu, "Evolutionary programming made faster," *IEEE Transactions on Computation*, Vol. 3, 82–102, 1999.
20. Ray, A., M. Kahar, S. Sarkar, S. Biswas, D. Sarkar, and P. P. Sarkar, "A novel broad and multiband frequency selective surface," *Microwave and Optical Technology Letters*, Vol. 54, 1353–1355, 2012.